

Chapter 5 CO oxidation over O-rich phases on Ru(10 $\bar{1}$ 0)

5.1 Motivation

The CO oxidation on Pt group metals such as Pd and Ir was suggested to be structure-insensitive, i.e., the catalytic activity is independent of different faces [115]. To study the structure sensitivity of the CO oxidation on RuO₂, other faces than (110) should be prepared.

On the Ru(0001) surface, which is flat and densely packed, incommensurate RuO₂(110) grows epitaxially along the high symmetric (10 $\bar{1}$ 0) direction under UHV conditions. Quite in contrast, the electrochemical preparation resulted in RuO₂ film oriented with the (100) face parallel to the Ru(0001) surface [116]. Also here, the RuO₂(100) film grows epitaxially and incommensurately [116]. Taking into account the lattice mismatch between RuO₂ films and the Ru(0001) substrate, one expects RuO₂(100) to be formed on Ru(0001), because the long side of RuO₂(100) matches the periodicity of the Ru(0001) in the (10 $\bar{1}$ 0) direction (4.69 Å) within 4.5 % (Fig. 5.1). However, as RuO₂ films grow incommensurately on the Ru(0001) surface, the corrugation of the potential energy surface of the underlying Ru(0001) substrate is obviously not sufficient to impose commensurability along the (10 $\bar{1}$ 0) direction. Thus, the lattice mismatch may not play a crucial role to judge the orientation of the RuO₂ film on Ru(0001). Recent DFT calculations revealed that the difference between the surface energy of RuO₂(110) (71 meV/Å²) and that of the (100) face (87 meV/Å²) is not very large [117], which may imply that the actual film orientation is governed only by kinetics.

In going to a more corrugated potential surface as that of Ru(10 $\bar{1}$ 0) (Fig. 5.2), the propensity to form lattice matched RuO₂ films at least along one direction may be higher due to the larger surface corrugation of Ru(10 $\bar{1}$ 0) than that of Ru(0001). The unit cell of Ru(10 $\bar{1}$ 0) is 3.11 Å×4.49 Å, while 3.11 Å×4.28 Å for RuO₂(100). The misfit between the long side of RuO₂(100) and the periodicity of Ru(10 $\bar{1}$ 0) along the [0001] direction (direction with the larger surface corrugation) is only 4.5 %.

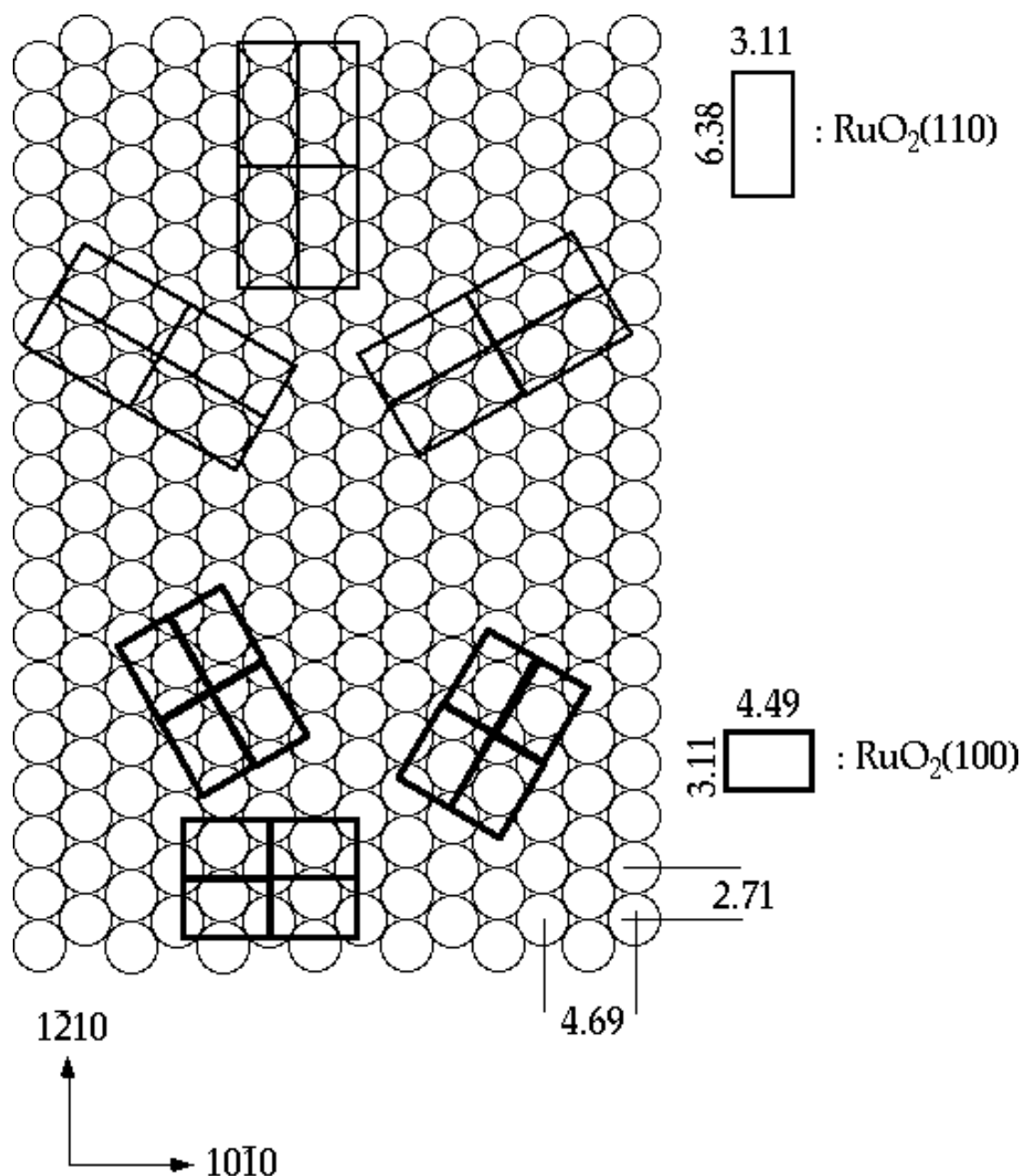


Fig. 5.1. Three rotational domains of $\text{RuO}_2(110)$ and $\text{RuO}_2(100)$ on $\text{Ru}(0001)$ are illustrated. The lattice mismatch between the long side of $\text{RuO}_2(100)$ along the $[10\bar{1}0]$ direction is only 4.5 %. The $\text{RuO}_2(100)$ lattice matches better with $\text{Ru}(0001)$ than $\text{RuO}_2(110)$. The values are given in Å.

Therefore, the $\text{RuO}_2(100)$ plane is expected to be exposed on $\text{Ru}(10\bar{1}0)$, which enables investigations of the structure sensitivity of the CO oxidation on RuO_2 . Thus, in this chapter we discuss O-rich phases on $\text{Ru}(10\bar{1}0)$.

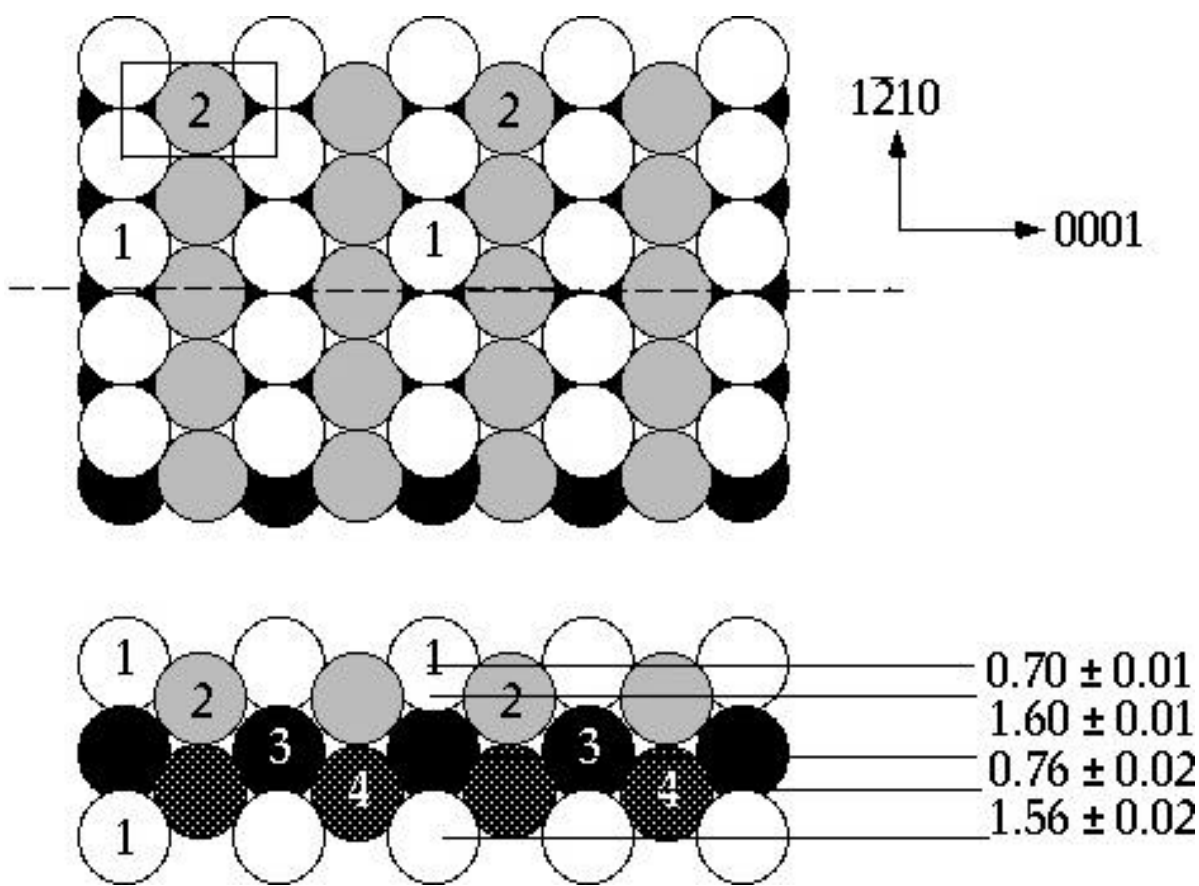


Fig. 5.2. Surface structure of the bare $\text{Ru}(10\bar{1}0)$ surface determined by LEED I/E analysis [26]. The values are given in \AA .

The $c(2\times 4)\text{-O}$ and $(2\times 1)\text{-p}2\text{mg-O}$ phases are formed at O coverages of 0.50 ML and 1.0 ML, respectively [73, 118, 119]. By exposing the $(2\times 1)\text{-p}2\text{mg-O}$ phase to NO_2 at 600 K, a (1×2) phase with streaky LEED spots appears at O coverages between 1–2 ML. An incommensurate structure appears at O coverages above 2–3ML [26]. No study was performed for the O-rich $\text{Ru}(10\bar{1}0)$ surfaces prepared with $\text{O}_2(\text{g})$ up to now.

5.2 Reactivity of O-rich phases on $\text{Ru}(10\bar{1}0)$ for CO oxidation

The averaged CO to CO_2 conversion probability on $\text{RuO}_2(110)/\text{Ru}(0001)$ is about

1 % [23]. To quantify the catalytic activity of O-rich Ru(10 $\bar{1}$ 0) surfaces towards CO oxidation, we performed CO titration experiments, the same procedure as used for determining the CO to CO₂ conversion probability on O-precovered Ru(0001) [23].

The Ru(10 $\bar{1}$ 0) sample was cleaned by cycles of sputtering with 1 kV at a sample temperature of 700 K and oxidation at 1000 K. 20 L of O₂ was dosed, and subsequently, a thermal desorption experiment was conducted. Sample cleaning was iterated, until the C+O recombination peak became negligibly small. The clean surface showed sharp spots and low background intensities in the LEED pattern.

The O-rich phases were prepared at a sample temperature of 760 K by exposing the bare Ru(10 $\bar{1}$ 0) to '6000 L' of O₂. The O uptake after this treatment was 57.8 ML. 5000 L of CO was exposed to these O-rich phases at various sample temperatures. Subsequently, O₂ thermal desorption experiments were performed to determine the O coverage left after CO exposures. One can estimate the amount of O reacted off during CO exposures. The results of these experiments are summarized in Fig. 5.3.

The CO to CO₂ conversion shows its maximum at a reaction temperature of 515 K. At this temperature, 43.3 ML of O atoms are reacted off by exposing 5000 L of CO.

We can estimate the averaged CO to CO₂ conversion probability of the O-rich Ru(10 $\bar{1}$ 0) surface. According to kinetic gas theory, the number of particles striking a surface of 1 cm² per second (n_s) is given by [29]

$$n_s = n_g \sqrt{\frac{RT}{2pM}} \quad (5.2.1)$$

where R is the gas constant, T is the absolute temperature, M is the molecular weight and n_g is the Avogadro number.

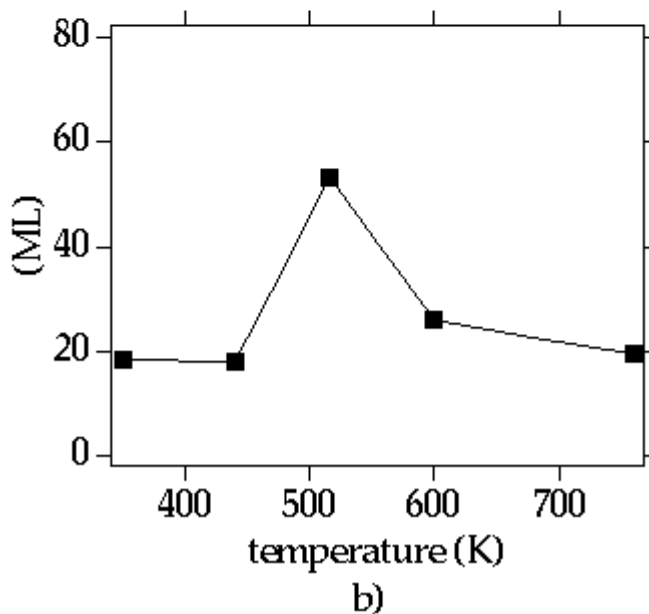
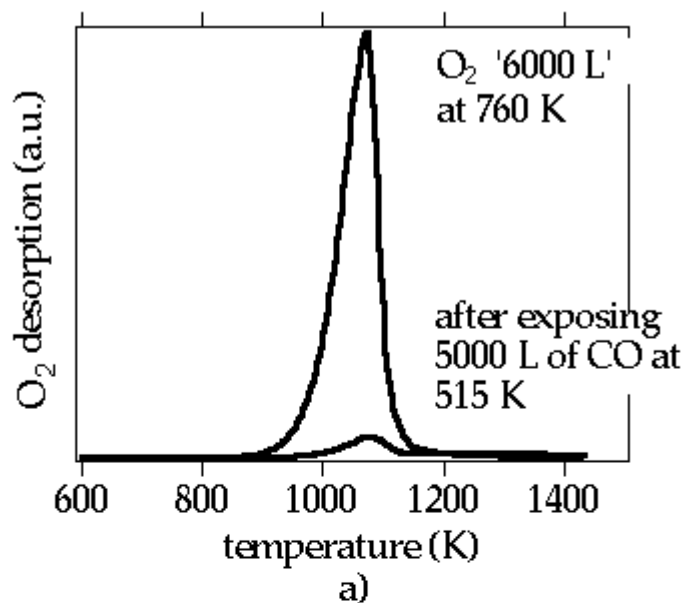


Fig. 5.3. a) TD spectra of the O-rich phase with an O coverage of 57.8 ML with and without postdosing CO at 515 K. The heating rate was 3 K/s. b) The y-axis indicates amounts of O reacted off during exposure of 5000 L of CO as a function of sample temperature.

The total number of CO molecules that strike the surface while exposing 5000 L of CO is 1.47×10^{18} molecule/cm² assuming the gas temperature to be 300 K. This corresponds to 1710 ML (the monolayer capacity of the Ru(10 $\bar{1}$ 0)

surface is $0.86 \times 10^{15}/\text{cm}^2$). The probability of CO to CO₂ conversion for the O- rich phases of Ru(10 $\bar{1}$ 0) at 515 K is then 2.5 %, which is comparable to that of the RuO₂(110)/Ru(0001).

At sample temperatures below 450 K or above 600 K, the probability of CO to CO₂ conversion is reduced. At lower temperatures, the O atoms on the surface are thermally less activated, resulting in lower CO to CO₂ conversion rates. Above 600 K, the O atoms are more activated. At higher temperatures, however, the residence time of CO on the surface is shorter than at lower reaction temperatures. The maximum reaction rate at about 500 K is the result of an optimum balance between the residence time of CO on the surface and the thermal activation of the O atoms at the surface.

5.3 O-rich phases prepared at 600 K

In Fig. 5.4, the thermal desorption spectra of the O phases of Ru(10 $\bar{1}$ 0) prepared at 600 K are depicted. After dosing '5 L' of O₂, the (2 \times 1)-p2mg-O appears. The O₂ desorption spectrum from a (2 \times 1)-p2mg-O phase shows a broad peak between 1100 K and 1450 K. The exposure of '400 L' of O₂ produces an additional peak at 1050 K. With LEED, a (1 \times 2) structure is visible. The LEED spots are streaky along the [0001] direction (Fig. 5.5a)). This indicates that the atomic distance along the [0001] direction is not well defined in this phase. Thus, we suggest that not only (1 \times 2), but also other (1 \times n) patches (n > 2, integer) coexist in this phase. The (2 \times 1)-p2mg-O overlayer beams cannot be observed anymore.

Exposing '6000 L' of O₂, the desorption peak at 1050 K shifts to a higher temperature, and an additional peak appears at about 1000 K. The LEED pattern shows a (0.86 \times 1) structure with low intensities in the LEED spots and high background intensities (Fig. 5.4b)). The size of the unit cell for the (0.86 \times 1) superstructure turns out to be 3.11 Å \times 4.28 Å. From the unit cells of the various low-index RuO₂ surfaces in Fig. 4.4, the (100) face (3.11 Å \times 4.49 Å) is the closest

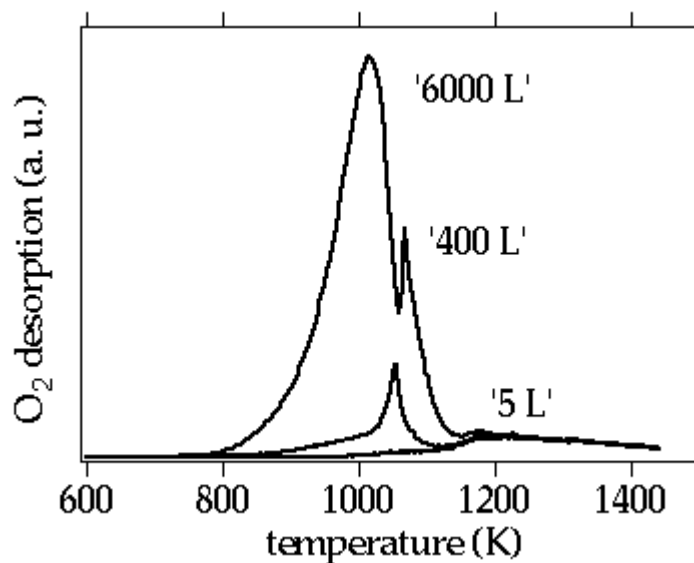


Fig. 5.4. TD spectra of O-rich phases prepared at 600 K. The heating rate was 3 K/s. The amounts of O₂ exposures are indicated. The quotation marks indicate that the shower system was used for dosing and amounts of exposures were estimated by reading background pressures during exposures.

to that of the oxide on Ru(10 $\bar{1}$ 0). Therefore, it is reasonable to assume that RuO₂(100) is grown on the Ru(10 $\bar{1}$ 0) surface. The unit cell of the RuO₂(100) is compressed in [010] direction with respect to the bulk RuO₂(100) by 4.5 %. It is interesting to note that a compression of 4.5 % along the [010] direction only marginally alters the Ru–O bond length in the bulk-truncated RuO₂(100) surface. This is very different from the RuO₂(110) surface. To compress the unit cell along the [001] and [$\bar{1}$ 10] directions, the Ru–O bond length changes more drastically, and therefore, this compression costs more energy. Recent DFT calculations have demonstrated that a uniform compression of the RuO₂(110) surface unit cell by 5 % causes the total energy to increase by about 1 eV, an enormous amount of energy that would be sufficient to burst the sample [120]. These observations are in good agreement with the large anisotropy in the linear compressibility of 2.6, i.e., the linear compressibility along the a-axis (Fig. 4.3) is by a factor of 2.6 smaller than along the c-axis [121].

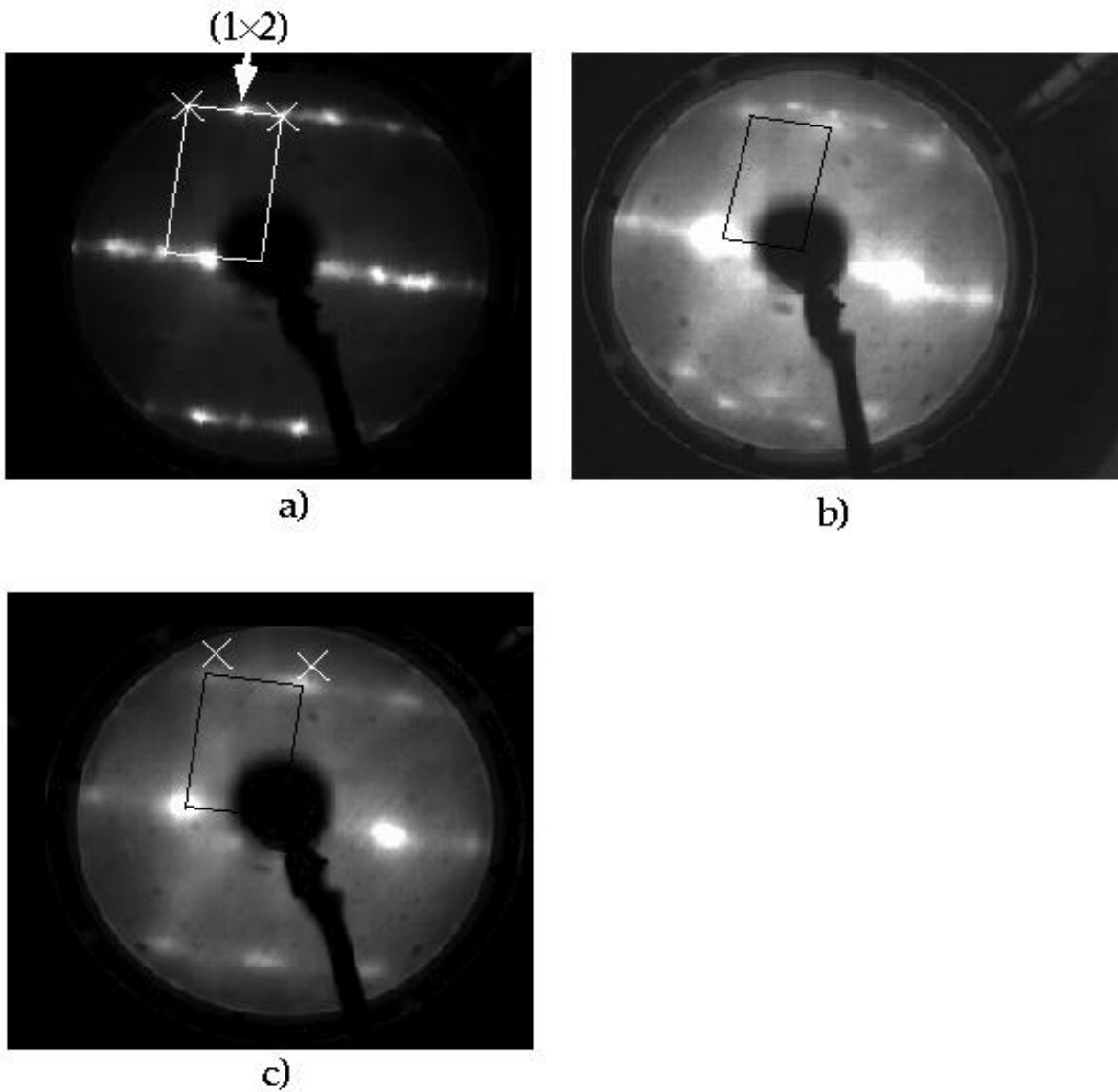


Fig. 5.5. LEED patterns for O-rich phases. a) After dosing ‘400 L’ of O_2 at 600 K. b) After dosing ‘6000 L’ of O_2 at 600 K. c) After dosing ‘6000 L’ at 660 K. The positions of the $\text{Ru}(10\bar{1}0)$ spots are marked with crosses.

Another interesting result is that the O_2 doses required for the preparation of oxide films on $\text{Ru}(10\bar{1}0)$ are much lower than on $\text{Ru}(0001)$. ‘6000 L’ of O_2 is sufficient to produce an oxide film on $\text{Ru}(10\bar{1}0)$, while at least ‘30000 L’ of O_2 is necessary to prepare $\text{RuO}_2(110)$ islands on $\text{Ru}(0001)$ at 600 K. These results are in line with the intuitive notion that more open surfaces can be more easily oxidized.

5.4 Formation of different oxide structures on Ru(10 $\bar{1}$ 0) at various preparation temperatures

To investigate structural changes of the oxide upon the preparation temperature, O-rich Ru(10 $\bar{1}$ 0) surfaces were produced by exposing '6000 L' of O₂ at various sample temperatures between 600 K and 770 K. Subsequently, thermal desorption spectroscopy (Fig. 5.6) and LEED (Fig. 5.5, 5.7) were employed to characterize these phases.

When a preparation temperature of 660 K was used, the shape of the TD spectrum is identical to that of 600 K, but the O uptake increased from 13 ML to 28 ML. The LEED pattern is identical to that of the O-rich phase prepared at 600 K, i.e., the (0.86 \times 1) phase, but exhibiting higher intensities of the LEED spots and lower

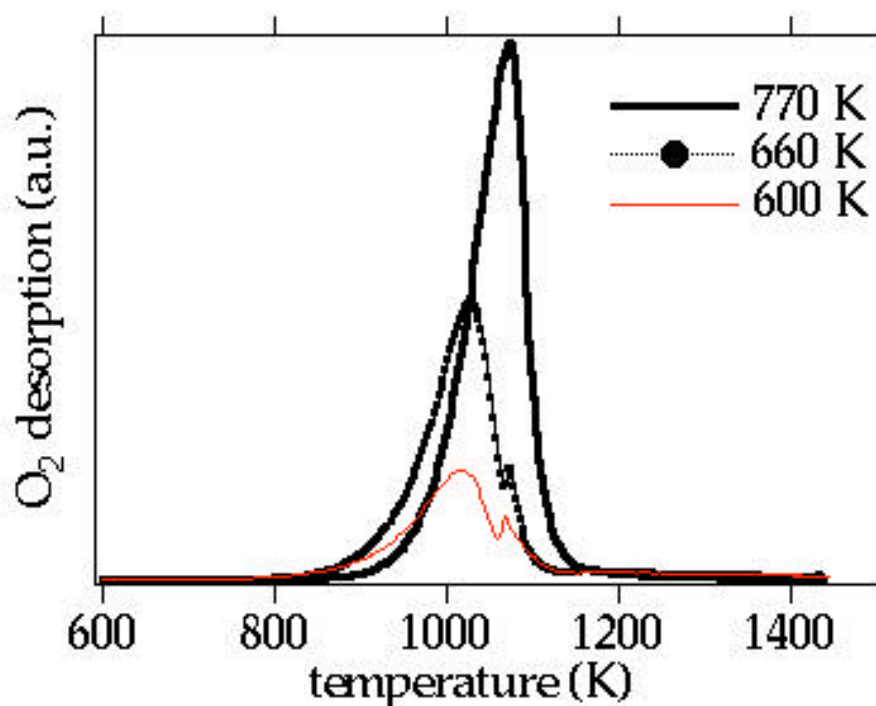


Fig. 5.6. TD spectra of O-rich phases on Ru(10 $\bar{1}$ 0) prepared with '6000 L' of O₂ at various sample temperatures. The heating rate was 3 K/s. The sample temperatures for the preparations are indicated.

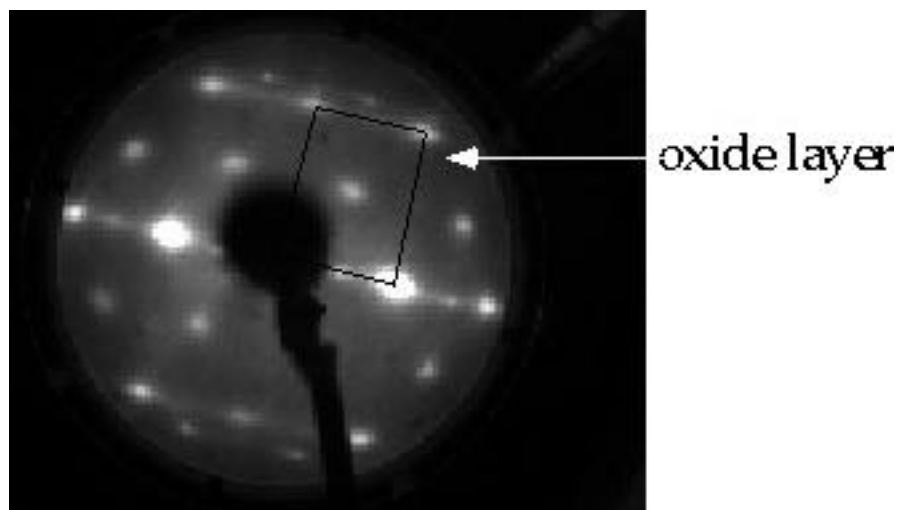


Fig. 5.7. LEED pattern for the O-rich phase prepared at 770 K. The unit cell of (0.86×1) is drawn on the picture. A $c(2 \times 2)$ superstructure with respect to the (0.86×1) structure is discernible.

background intensities (Fig. 5.5 c)). The (1×2) structure is not visible in the LEED pattern.

At a preparation temperature of 770 K, both the onset of O_2 desorption and the desorption peak shift to higher temperatures (Fig. 5.6). The LEED pattern shows a $c(2 \times 2)$ superstructure with respect to the oxide film with a (0.86×1) periodicity (Fig. 5.7). Previous studies reported that the (110) and (100) planes of bulk RuO_2 are reconstructed to $c(2 \times 2)$ or (1×2) structures by annealing at above 700 K under UHV conditions or moderate O_2 atmosphere [112]. In this work, no surface reconstruction of $RuO_2(110)$ was found, whereas the $RuO_2(100)$ surface is converted into a $c(2 \times 2)$ structure at a preparation temperature of 770 K.

5.5 Adsorption of CO on (1×1) - $RuO_2(100)/Ru(10\bar{1}0)$

After the preparation of $RuO_2(100)/Ru(10\bar{1}0)$ by exposing '6000 L' of O_2 at 660 K, 100 L of CO was dosed at a sample temperature of 100 K. The LEED I/E curves before and after CO exposure are compared in Fig. 5.8. The LEED I/E curves changed

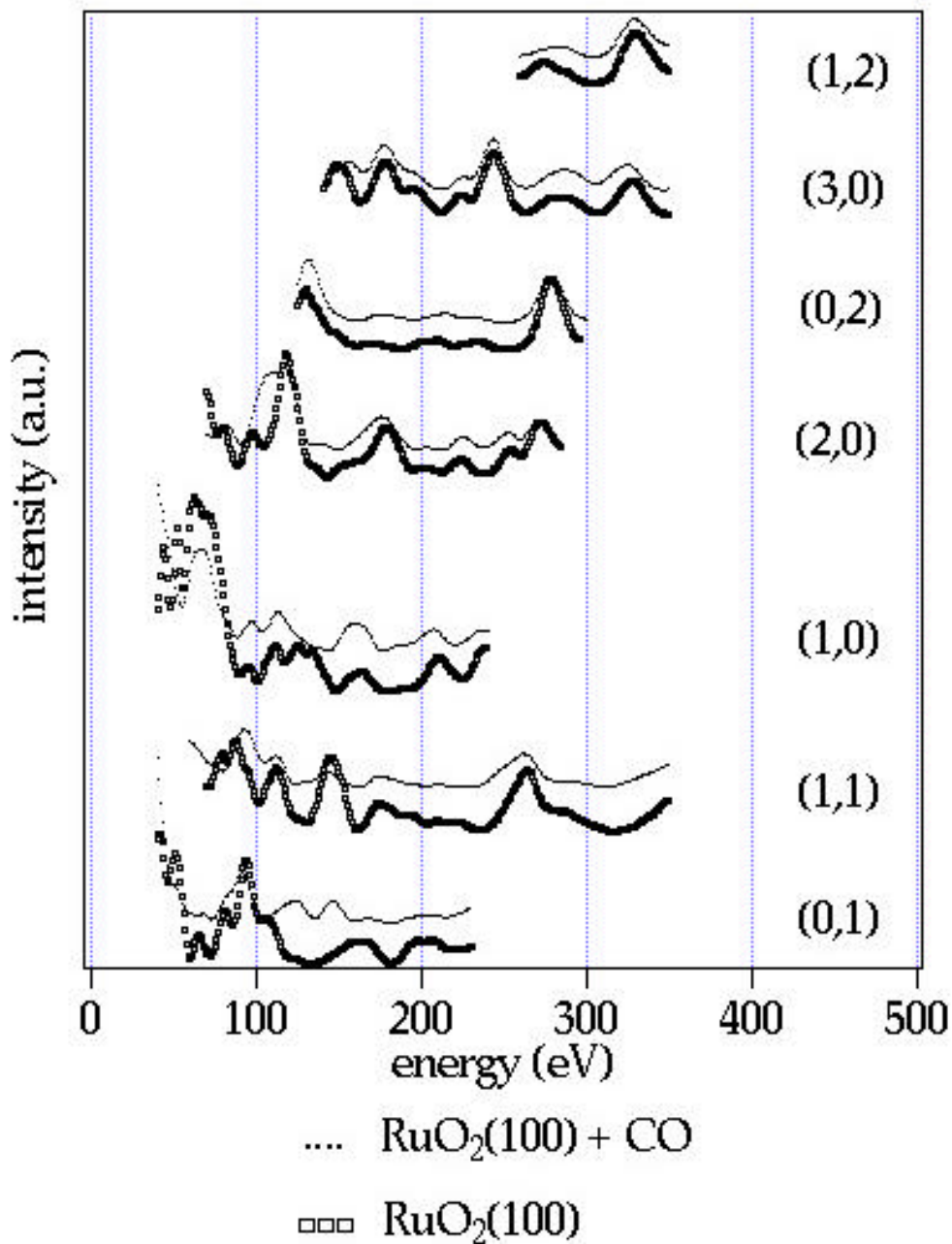


Fig. 5.8. The LEED I/E curves of $\text{RuO}_2(100)/\text{Ru}(10\bar{1}0)$ before and after dosing 100 L of CO at 100 K are compared ($R_p = 0.28$).

significantly upon exposing to CO ($R_p = 0.28$). Consequently, CO molecules adsorb on specific sites over $\text{RuO}_2(100)/\text{Ru}(10\bar{1}0)$. The CO molecules on $\text{RuO}_2(100)/\text{Ru}(10\bar{1}0)$ desorb between 200 K and 600 K. With CO, desorption signals of CO_2 are also detectable between 200 K and 350 K (Fig. 5.9).

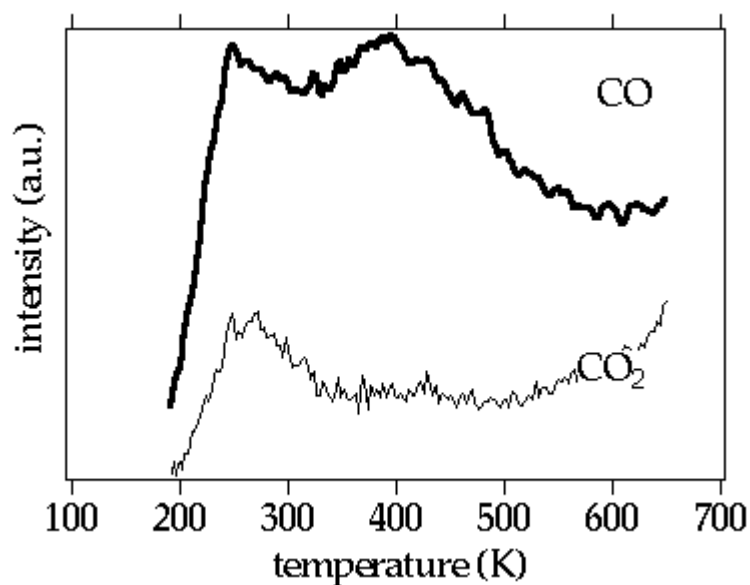


Fig. 5.9. TD spectra of CO and CO₂ from the RuO₂(100)/Ru(10 $\bar{1}$ 0) after exposing 10 L of CO at 200 K. The heating rate was 3 K/s.

The results of the thermal desorption experiments (Fig. 5.4 for O₂ desorption, Fig. 5.9 for CO and CO₂) are similar to those of RuO₂(110) on Ru(0001). Since an additional O₂ desorption state appears at 1000 K with the RuO₂(100) formation, heating the O-rich Ru(10 $\bar{1}$ 0) to 1000 K removes most of the lattice oxygen in the RuO₂(100) film, leaving chemisorbed O atoms. This indicates that the lattice O atoms of the RuO₂(100) film are more loosely bound than the chemisorbed O atoms on the Ru(10 $\bar{1}$ 0) surface. On the other hand, the binding energy of CO on RuO₂(100)/Ru(10 $\bar{1}$ 0) is high, as indicated by the high desorption temperature. Therefore, RuO₂(100) should be responsible for the high activity of O-rich Ru(10 $\bar{1}$ 0) surfaces for CO oxidation.

5.6 Atomic surface structure of (1×1)-RuO₂(100)/Ru(10 $\bar{1}$ 0)

We discuss the atomic surface structure of RuO₂(100). Three essentially different models are envisioned for the RuO₂(100) surface: A: Ru termination, B: exposing

bridging O array and cus Ru atoms, C: onefold coordinated O termination (Fig. 5.10). These three models were tested in the LEED I/E calculations. From recent STM investigations, the defect-free and homogeneous (1×1)-RuO₂(100) surface was observed on the O-rich Ru(10 $\bar{1}$ 0) surface [122]. Consequently, we can rule out any mixed surface structures as (A+B), (B+C) or (A+C) for the RuO₂(100)/Ru(10 $\bar{1}$ 0) surface.

The LEED I/E curves of eight symmetrically non-equivalent beams from the (0.86×1) structure were collected with the total energy range of 1408 eV. The vertical positions of the onefold coordinated O, the bridging O and the atoms in the first Ru plane, the first O bilayer, the second Ru plane and the second O bilayer were refined in the LEED I/E analysis. The vertical distances in deeper layers were assumed to be 5 % expanded with respect to the bulk value so that the volume of the unit cell is conserved and fulfills the Liouville theorem. However, the error bar for atomic positions in these deeper layers is larger than 0.1 Å. Thus, we cannot discriminate, if the vertical distances in deeper layers are really expanded with respect to the bulk values or not. The lateral positions of onefold coordinated O and bridging O were also relaxed in the fit procedure. The Debye temperatures of the onefold coordinated O, the bridging O and the first plane Ru were refined. The Debye temperatures of O and Ru in deeper layers were fixed at 600 K and 420 K, respectively.

The LEED I/E calculations with the bridging O termination (model B) and onefold O terminations (model C) gave satisfying agreements between theory and experiment ($R_p = 0.33$, respectively). The Ru terminated surface (model A) can be excluded due to a worse agreement between experiment and theory ($R_p = 0.41$) than models of bridging O termination and onefold coordinated O termination.

To discriminate between the terminations by onefold coordinated O and bridging O, RuO₂(100)/Ru(10 $\bar{1}$ 0) was exposed to ‘100 L’ of O₂ at a sample temperature of 300 K. The I/E curves were collected before and after O₂ exposure (Fig. 5.11).

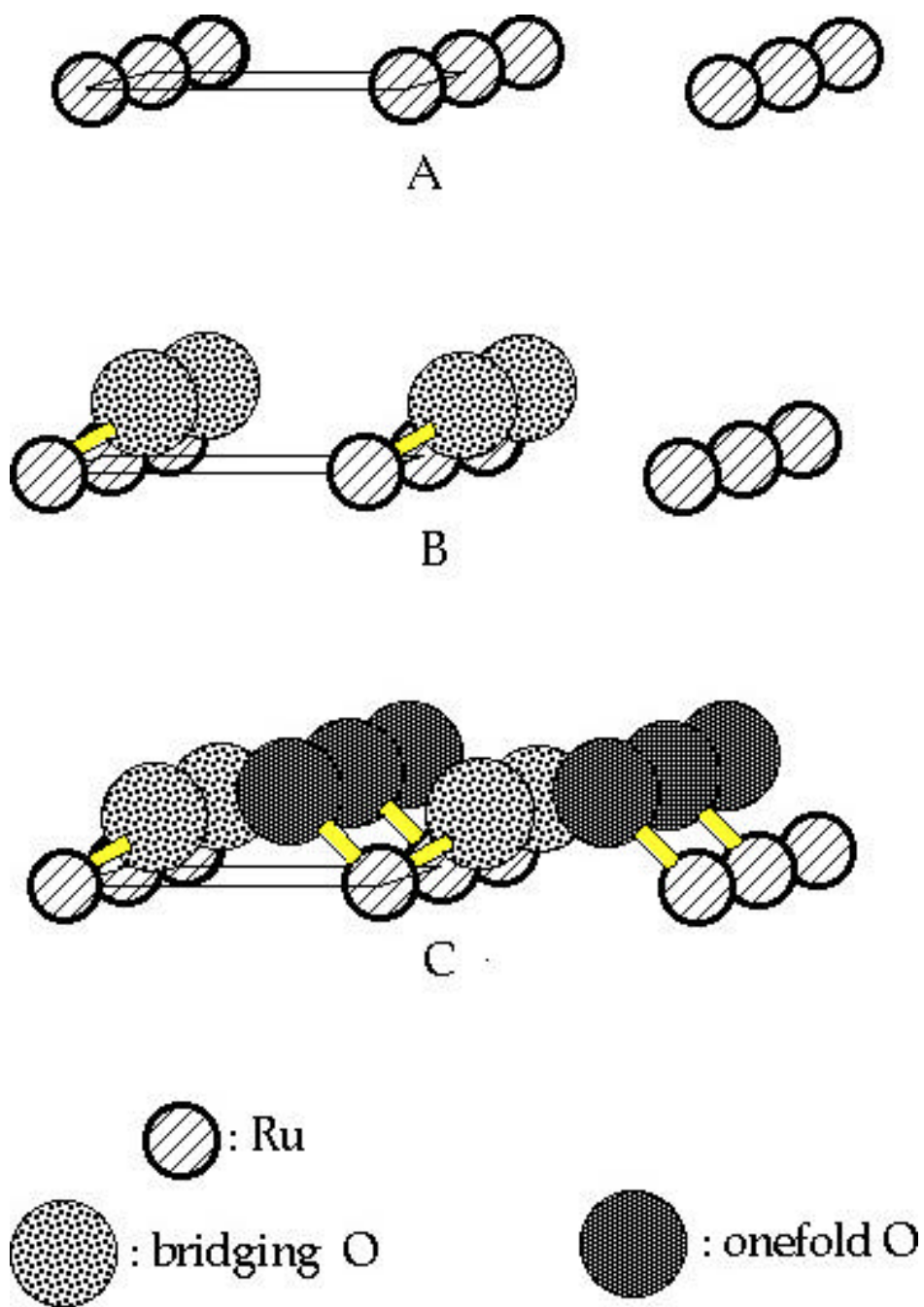


Fig. 5.10. Possible terminations of $\text{RuO}_2(100)$. A: Ru termination. B: twofold O termination. C: onefold O termination.

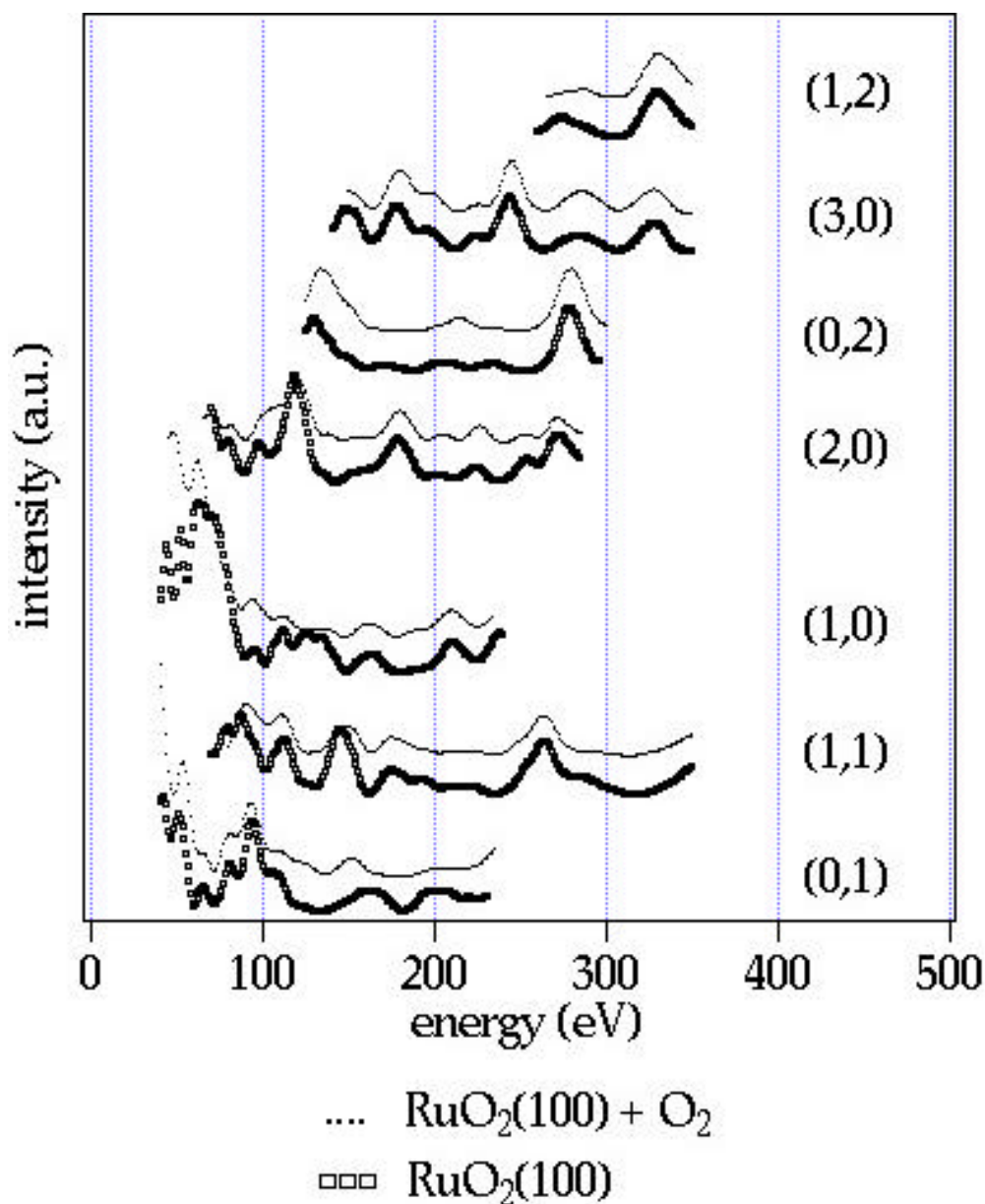


Fig. 5.11. The LEED I/E curves of $\text{RuO}_2(100)/\text{Ru}(10\bar{1}0)$ collected before and after dosing '100 L' of O_2 at 300 K are compared ($R_p = 0.18$).

The LEED I/E curves alter significantly after O_2 exposure. R_p between the I/E curves of $\text{RuO}_2(100)/\text{Ru}(10\bar{1}0)$ measured before and after O_2 exposure is 0.18. Consequently, O_2 adsorption on $\text{RuO}_2(100)/\text{Ru}(10\bar{1}0)$ is allowed, which implies the presence of the cus Ru atoms on the surface. Thus, we conclude that the $\text{RuO}_2(100)/\text{Ru}(10\bar{1}0)$ surface exposes both bridging O array and cus Ru atoms consistent

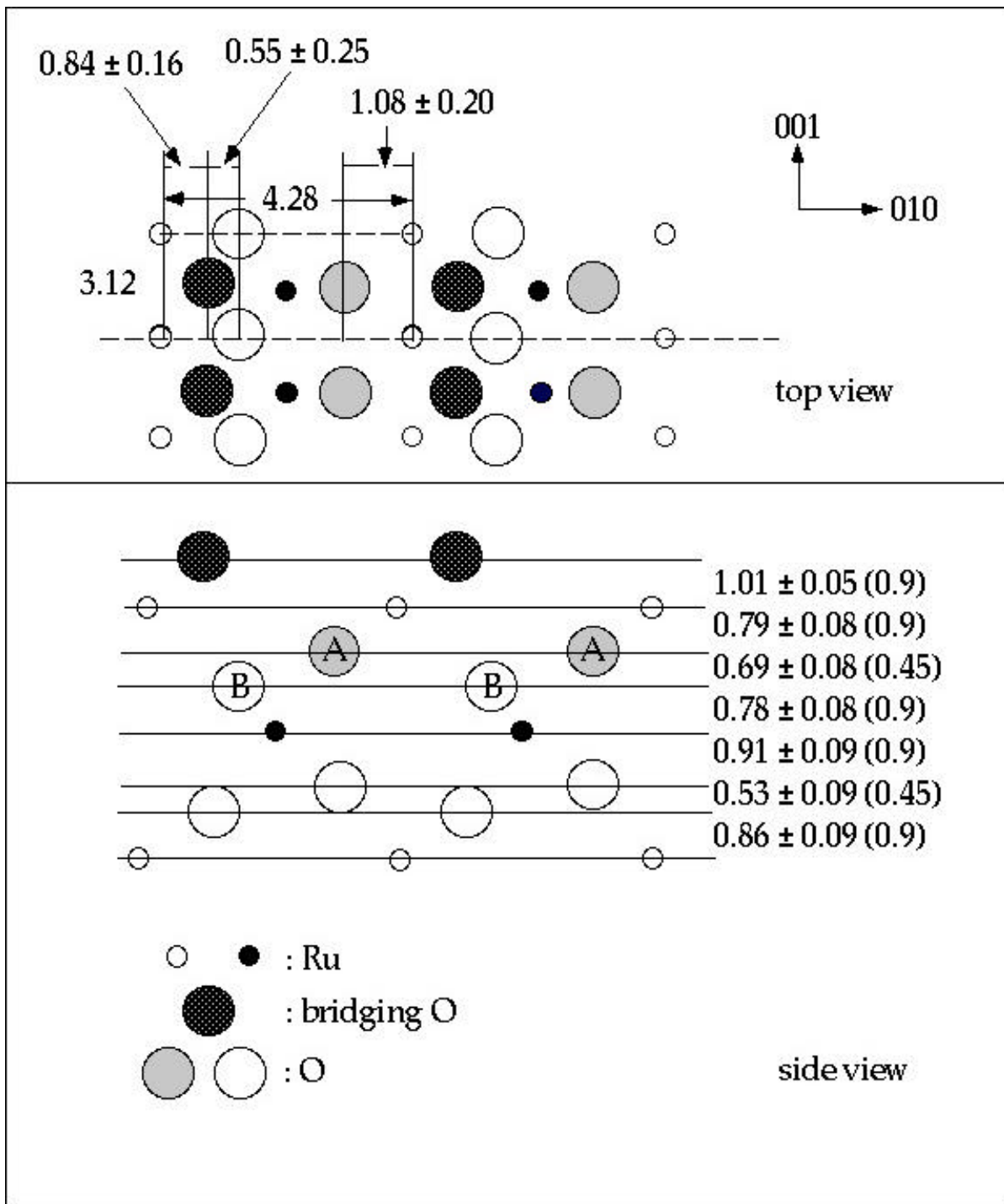


Fig. 5.12. Best-fit structure of $\text{RuO}_2(100)$ on $\text{Ru}(10\bar{1}0)$ determined by a LEED I/E analysis. The bulk values of the atomic positions are given in parentheses. The values are given in Å.

with model B, but not consistent with model C. The CO adsorption on $\text{RuO}_2(100)/\text{Ru}(10\bar{1}0)$ is also a supportive evidence for model B.

The best-fit structure for the bridging O terminated $\text{RuO}_2(100)/\text{Ru}(10\bar{1}0)$ surface is shown in Fig. 5.12. O(A) is lifted upwards to the first Ru plane, while O(B) is moved downwards to the second Ru plane with respect to the bulk positions. Since $\text{RuO}_2(100)$ is compressed laterally in one direction ([010] direction),

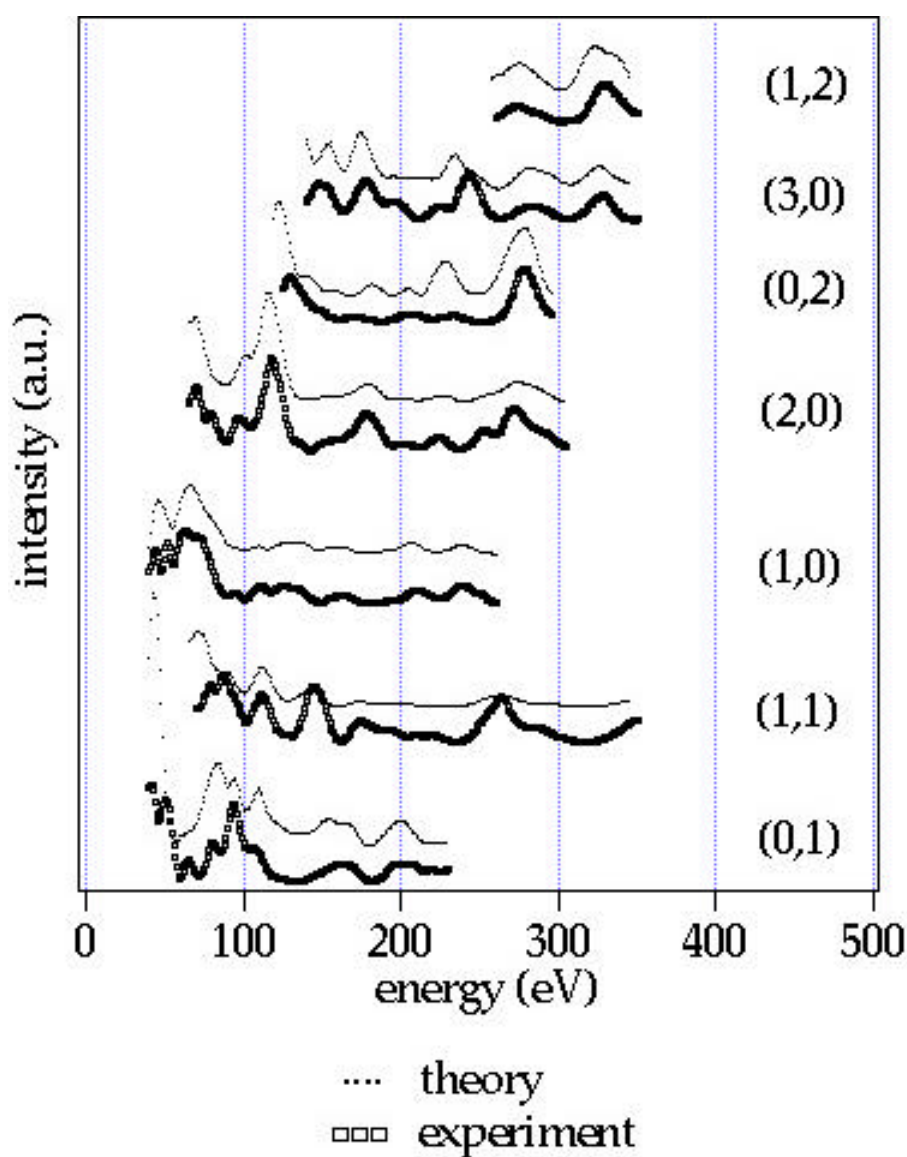


Fig. 5.13. The experimental LEED I/E curves and the calculated ones for the best-fit structure of $\text{RuO}_2(100)/\text{Ru}(10\bar{1}0)$ are compared. ($R_p = 0.33$).

the expansion of the vertical parameters is expected to preserve bulk-like bond distances between the atoms. In fact, the distance between the second and the third Ru layer is 2.32 Å, which is expanded by 3 % with respect to the bulk value. However, the distance between the first and the second Ru layer is identical to the bulk value. Ru–O (bridging) bond length is 2.01 Å, which is the same as the bulk value (2.01 Å).

In Fig. 5.13, the experimental and calculated LEED I/E curves for the best-fit structure of RuO₂(100)/Ru(10 $\bar{1}$ 0) terminated by bridging O arrays are reproduced.

5.7 Adsorption of CO on c(2×2)-RuO₂(100)/Ru(10 $\bar{1}$ 0)

After the c(2×2)-RuO₂(100) film had been exposed to 100 L of CO at 100 K, the I/E curves were measured (Fig. 5.14). No change of the fractional-order beams can be observed by exposing to CO. Neither the shape nor the absolute intensities of the fractional-order beams show any change. The integer-order beams change significantly upon dosing CO.

The only model, which can explain these experimental observations, is the following: The (1×1) and the c(2×2) structure of RuO₂(100) coexist on the O-rich phase prepared at a sample temperature of 770 K, and CO molecules adsorb selectively on the (1×1)-RuO₂(100) domains. Therefore, we suggest that no cus Ru atoms are present on the c(2×2)-RuO₂(100).

We demonstrated in this chapter that RuO₂(100) allows CO adsorption at room temperature and that therefore RuO₂(100) should be active for CO oxidation. However, CO does not adsorb on c(2×2)-RuO₂(100). These results imply that CO adsorption on RuO₂ is sensitive to the actual surface structure. We propose that cus Ru atoms should be present at the RuO₂ surface to enable CO oxidation with substantially high reaction rates.

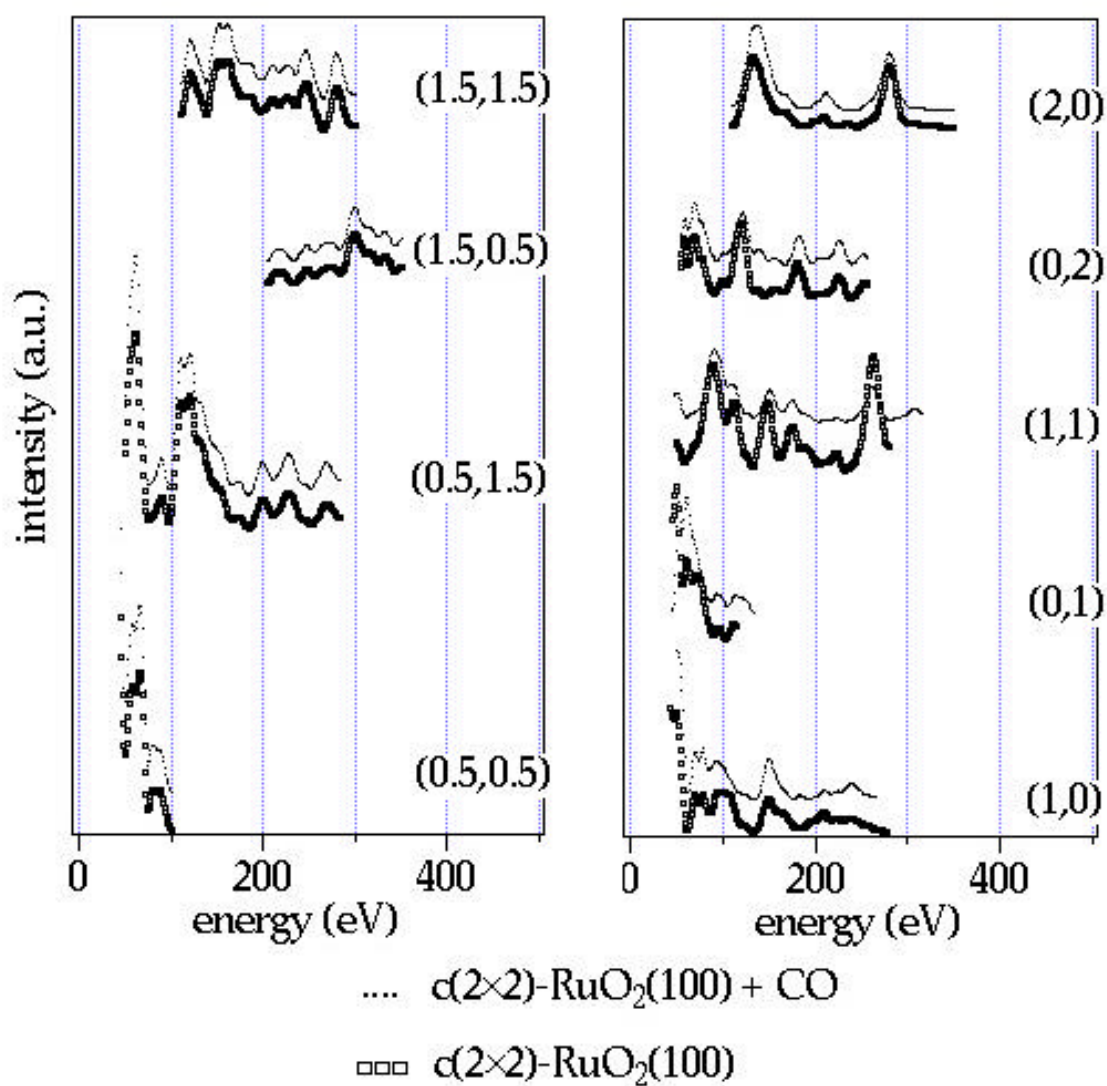


Fig. 5.14. The LEED I/E curves of the $c(2 \times 2)$ structure of $\text{RuO}_2(100)$ on $\text{Ru}(10\bar{1}0)$ before and after exposing to CO at 110 K. R_p between the integer-order beams of the two data sets is 0.28, while $R_p = 0.01$ for fractional-order beams.